Geomechanics and Engineering, *Vol. 34, No. 4 (2023) 409-424*
https://doi.org/10.12989/gae.2023.34.4.409

Response of steel pipeline crossing strike-slip fault in clayey soils by nonlinear analysis method

Hadi Khanbabazadeh*[1] and Ahmet Can Mert[2]

[1]*Department of Engineering, Gebze Technical University, Kocaeli, Turkey*
[2]*Department of Civil Engineering, Istanbul Kutlur University, 34158 Istanbul, Turkey*

(*Received April 8, 2023, Revised June 25, 2023, Accepted July 6, 2023*)

Abstract. Response of the pipeline crossing fault is considered as the large strain problem. Proper estimation of the pipeline response plays important role in mitigation studies. In this study, an advanced continuum modeling including material non-linearity in large strain deformations, hardening/softening soil behavior and soil-pipeline interaction is applied. Through the application of a fully nonlinear analysis based on an explicit finite difference method, the mechanics of the pipeline behavior and its interaction with soil under large strains is presented in more detail. To make the results useful in oil and gas engineering works, a continuous pipeline of two steel grades buried in two clayey soil types with four different crossing angles of 30°, 45°, 70° and 90° with respect to the pipeline axis have been considered. The results are presented as the fault movement corresponding to different damage limit states. It was seen that the maximum affected pipeline length is about 20 meters for the studied conditions. Also, the affected length around the fault cutting plane is asymmetric with about 35% and 65% at the fault moving and stationary block, respectively. Local buckling is the dominant damage state for greater crossing angle of 90° with the fault displacement varying from 0.4 m to 0.55 m. While the tensile strain limit is the main damage state at the crossing angles of 70° and 45°, the cross-sectional flattening limit becomes the main damage state at the smaller 30° crossing angles. Compared to the stiff clayey soil, the fault movement resulting 3% tensile strain limit reach up to 40% in soft clayey soil. Also, it was seen that the effect of the pipeline internal pressure reaches up to about 40% compared to non-pressurized condition for some cases.

Keywords: buried steel pipes; continuous pipelines; fault crossings; nonlinear soil behavior; soil-pipe interaction; strick-slip fault

1. Introduction

Buried pipelines pass seismically active lands and cross through active faults. Transient ground deformation (TGD) and permanent ground deformation (PGD) are two main damage sources for segmented and continuous pipelines. While few damages under the effect of the wave propagation have been reported (O'Rourke and Liu 1999, Hashash *et al.* 2001, O'Rourke 2009, Yigit 2022, Shi *et al.* 2022, Xu and She 2022), the active faults in the seismic areas have been proven to be the most challenging geological hazards facing by the long-distance gas and oil pipelines (MaCaffrey and O'Rourke 1983, Desmod *et al.* 1995, Kokavessis and Anagnostidis 2006, Ozcebe *et al.* 2015, Karamanos *et al.* 2014, Erenson and Terzi 2022).

As the pioneers, Newmark and Hall (1975) developed simplified analysis methods for the pipelines subjected to fault crossing condition. Then, based on the elastic foundation theory, Kennedy *et al.* (1977) proposed a closed form solution for the soil-pipe interaction (SPI) problem. Because of the neglecting of the flexural rigidity of the pipe in this work, Wang and Yeh (1985) developed an analytical methodology by considering pipeline bending stiffness.

Since then, several analytical methods have been proposed by other researchers for soil-pipe interaction problems (SPI) (Sarvanis and Karamanos 2017, Talebi and Kiyono 2021, Karamitros *et al.* 2011, Trifonov and Cherniy 2012). Karamitros *et al.* (2007) proposed an analytical method based on the beam on the elastic foundation. To extend the application area of the analytical models in the pipeline design, Trifonov and Cherniy (2010) presented a semi-analytical methodology for the nonlinear stress-strain analysis of the buried steel pipelines. Although such methods could present approximate results for certain cases, they lack the proper consideration of the SPI. Generally, two types of models are considered for SPI analyses; The beam-type model and the continuum model (Tohidi and Shakib 2003, Karamanos *et al.* 2014). Several examples of the application of the beam-type model exist in the literature (Toprak *et al.* 2010, Joshi *et al.* 2011). Melissianos and Gantes (2017) modeled the pipeline by the beam-type finite elements (FE), while the soil was presented by a series of mutually independent translational non-linear springs in three directions. In another study, Roudsari *et al.* (2019) presented an optimization algorithm for the calculation of the stiffness of the equivalent transverse spring of the sandy soil in the beam-type modeling. Application of Meshfree Methods (MM) in the modeling of geomaterial and discontinuities at large strains would also be another technique for such problems (Khoshghalb *et al.* 2020, Shafee, and Khoshghalb 2021, 2022, Salehi Dezfooli *et al.* 2022).

*Corresponding author, Assistant Professor
E-mail: hk.babazadeh@gtu.edu.tr

http://www.techno-press.org/?journal=gae&subpage=7
ISSN: 2005-307X (Print), 2092-6219 (Online)

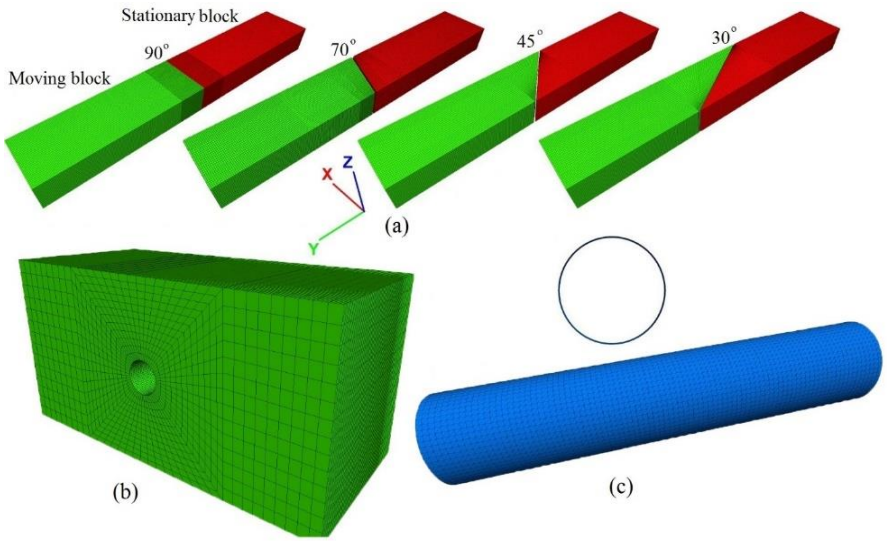

Fig. 1 Numerical models of the pipeline crossing fault: (a) longitudinal finite difference mesh for soil, (b) cross-sectional finite difference mesh for soil and (c) finite element (pipeline) mesh and pipe cross section

To see the effects of factors like SPI, material non-linearity and large geometric deformations, the consideration of the problem using continuum modeling is inevitable (Takada *et al.* 1998, Liu *et al.* 2004, Liu *et al.* 2008, Vazouras *et al.* 2010, Chaudhari *et al.* 2013, Akbas *et al.* 2015, Trifonov 2015, Vazouras and Karamanos 2017). In this regard, Morshed *et al*. (2020) investigated the behavior of the pipeline buried in dense sand considering the pre-peak hardening, post-peak softening, density, and confining pressure dependent behavior of sand. Dey *et al.* (2020) studied the structural response of buried continuous pipeline undergoing strike-slip fault rupture using FE model including both material and geometric nonlinearities. Vazouras *et al.* (2015) and Kaya *et al.* (2015) studied the interaction of the surrounding soil using a contact algorithm through a friction coefficient. To eliminate some of the disadvantages of the continuum-based modeling approach, Banushi *et al.* (2018) introduced an innovated analysis in which both soil and pipe contact surfaces are meshed with a similar mesh size guaranteeing solution convergence. Methods other than FE have also been used by the researchers. Rahman and Taniyama (2015) applied distinct element method analyze of a buried pipeline subjected to fault displacement. Despite the drawbacks of its application for different soil types, Shokouhi *et al.* (2013) proposed the hybrid FE-Artificial Neural Network (ANN) approach for seismic strain analysis of high-density polyethylene (HDPE) pipelines.

The response of the pipeline crossing fault is considered as the large strain problem. For such problems, the interaction of the structural element under constrained conditions with surrounding soil is the determining factor. The successful application of these details will affect the accuracy of the modeling results. In this study, the mechanical behavior of the continuous steel pipeline crossing strike-slip fault is investigated by a fully nonlinear method based on explicit finite difference scheme (Cundall 2008). In this formulation, the incremental displacements of the continua are added to the coordinates so that the grid moves and deforms with the material that it represents. The behavior of the soil is modeled by a proper elasto-plastic constitutive model with a hardening and non-associated flow rule. Also, the softening behavior of the surrounding soil has been considered as well. The interaction between the shell-type structural element is implemented through an advanced scheme considers both normal-directed compressive/tensile and shear-directed frictional interaction as well as sliding and separation at large strain conditions. In this way, the mechanics of the pipeline behavior and its interaction with soil under large strain level is presented in more detail.

2. Analysis method

The proper modeling of the SPI, especially in the large strain problems, affects the modeling results' accuracy. To this end, a robust analysis method is necessary. In contrast to the ordinary Eulerian formulation, in which the material moves and deforms relative to a fixed grid, in the used Lagrangian formulation the incremental displacements are added to the coordinates so that the grid moves and deforms with the material it represents. In this way, the movement of each mesh zone occurs with higher accuracy in the problems with large mesh displacements. The continuum is modeled by constant strain-rate tetrahedra element. Soil behavior is modeled by a proper elasto-plastic constitutive model with non-associated flow rule for shear failure, and an associated rule for tension failure has been utilized. Both hardening and softening behaviors are included in the used constitutive model. Also, using a set of interaction springs in normal and tangent directions the friction, sliding and separation between host medium and structural elements are modeled with high accuracy. The solution of the full equations of motions are performed by a fully nonlinear method using FLAC3D code. More explanations on the above-mentioned items are presented in the following sections.

Table 1 The geotechnical properties of the used soil types

Soil classification		c (kPa)	∅ (°)	V_s (m/s)	G (kPa)	K (kPa)	γ (kN/m^3)	PI(%)
Clay	stiff	75~90	10	200~400	0.76e5~3.36e5	2e5~8.8e5	19~21	30
	Soft	34~45	10	75~175	10.1e3~61.2e3	26.4e3~159.7e3	18-20	10

∅ : internal friction angle; c: cohesion; V_s: shear wave velocity; G: shear modulus; K: bulk modulus; γ: unit weight

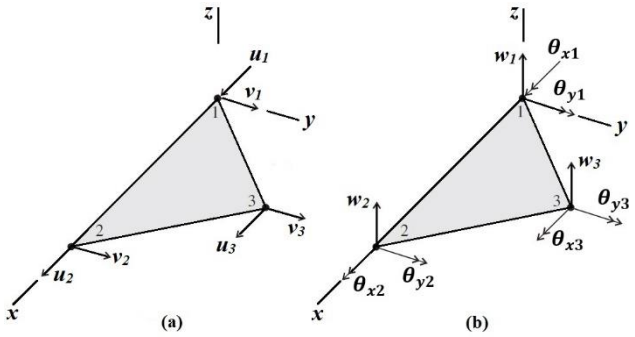

Fig. 2 Nodal DOFs of the structural element (local system): (a) membrane action and (b) bending action

2.1 Fault model specification and material properties

The numerical models comprise two soil blocks each of which is 30 m length (60 m in total), 10 m width and 5 m height, as shown in Fig. 1. The depth of the pipeline was selected with respect to the usual approximate depth applied in practice (Mohitpour *et al.* 2007, Vazouras *et al.* 2010, Vazouras *et al.* 2012). The strike-slip fault cutting plane is assumed perpendicular to the pipeline axis at the middle of the pipe length, representing the vertical fault plane. An irregular mesh size has been applied in longitudinal direction. Four different crossing angles of 30°, 45°, 70° and 90° with respect to the pipeline axis have been considered.

To investigate the embedded soil effect, two soil types of soft and stiff clays are considered (Table 1). As the soil behavior, a proper elasto-plastic constitutive model is utilized. Its failure envelope corresponds to the Mohr-Coulomb criterion (shear yield function) with tension cutoff (tensile yield function). The shear flow rule is non-associated for compression and associated to the tensile. Both hardening and softening behaviors are included. The softening behavior is done by integrating additional formulation to FLAC's standard elasto-plastic Mohr-Coulomb model. To do that, the cohesion and friction have been defined as piecewise-linear softening law for the tensile strength in terms of another hardening parameter measuring the plastic tensile strain.

2.2 Soil-pipe interaction modeling

The embedded continuous pipeline is modeled by the liner structural element. It is an advanced DKT-CST (Discrete Kirchhoff Theory-Constant Stress Triangle) shell-type structural element with both normal-directed compressive/tensile and shear-directed frictional interaction with the surrounding soil (Cook *et al.* 1989). To consider proper SPI, its mesh size has been chosen less than 1/26 of the pipeline outer diameter (D) (Vazouras *et al.* 2012). Both soil and pipe contact surfaces are meshed with a similar mesh size guaranteeing solution convergence. The nodal DOFs for an element in the xy-plane in the local coordinate system is shown in Fig. 2.

$$\{\mathbf{d}\} = \lfloor \mathbf{u}_i \ \mathbf{v}_i \ \mathbf{w}_i \ \boldsymbol{\theta}_{xi} \ \boldsymbol{\theta}_{yi} \rfloor^T \tag{1}$$

where

$$\lfloor \mathbf{u}_i \rfloor = \lfloor u_1 \ u_2 \ u_3 \rfloor, \quad \lfloor \mathbf{v}_i \rfloor = \lfloor v_1 \ v_2 \ v_3 \rfloor, \quad \lfloor \mathbf{w}_i \rfloor = \lfloor w_1 \ w_2 \ w_3 \rfloor$$
$$\lfloor \boldsymbol{\theta}_{xi} \rfloor = \lfloor \theta_{x1} \ \theta_{x2} \ \theta_{x3} \rfloor, \quad \lfloor \boldsymbol{\theta}_{yi} \rfloor = \lfloor \theta_{y1} \ \theta_{y2} \ \theta_{y3} \rfloor \tag{2}$$

The stiffness matrix of the DKT-CST shell element in local xyz coordinates is presented by [**k**]

$$[\mathbf{k}]\{\mathbf{d}\} = \begin{bmatrix} [\mathbf{k}_{CST}]_{6\times6} & [0]_{6\times9} \\ [0]_{9\times6} & [\mathbf{k}_{DKT}]_{9\times9} \end{bmatrix} \begin{Bmatrix} \mathbf{u}_i \\ \mathbf{v}_i \\ \mathbf{w}_i \\ \boldsymbol{\theta}_{xi} \\ \boldsymbol{\theta}_{yi} \end{Bmatrix} \tag{3}$$

where $[k_{CST}]$ and $[k_{DKT}]$ are the stiffness matrixes of CST and DKT plate bending element, respectively. This element is attached to the surface of the surrounding finite difference mesh through the nodes of the structural element.

The idealization of the interface behavior at a liner node is shown in Fig. 3. Also, the normal and shear directed behavior of the liner-zone interface as well as its frictional and cohesive nature are schematically presented in Fig. 4.

In order to make the results useful in practice, two steel types of API 5L X65 and X80 with two typical pipe wall thicknesses of 1/4in (6.35 mm) and 1/2in (12.7 mm) corresponding to D/t ratio of 144 and 72 are used. The outer diameter of the pipeline is 914.4 mm (36in.). Fig. 5 shows the nominal stress-strain behavior of the API 5L X65 and X80 steel types (ANSI/API Spec 5L 2007, Anastasopoulos *et al.* 2007).

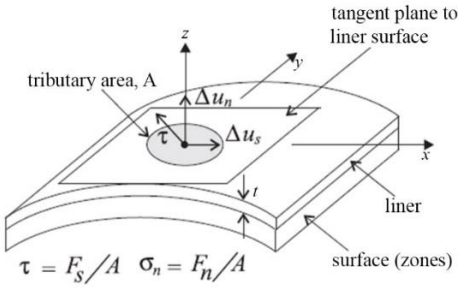

Fig. 3 Idealization of the interface behavior at a node

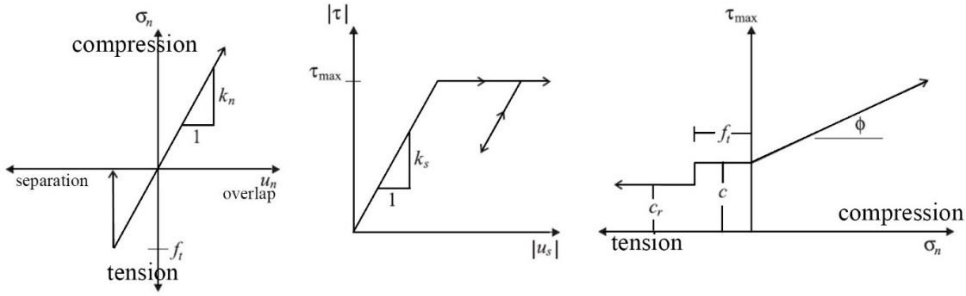

Fig. 4 Schematic presentation of (a) normal and (b) shear directed interaction at a liner-zone interface

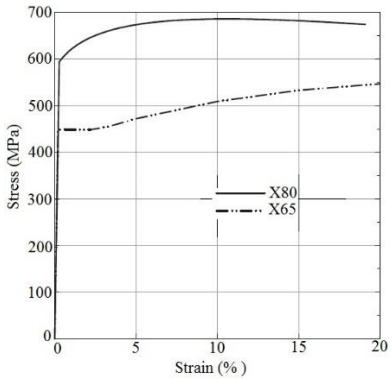

Fig. 5 Nominal stress-strain behavior of the API 5L X65 and X80 steel pipe

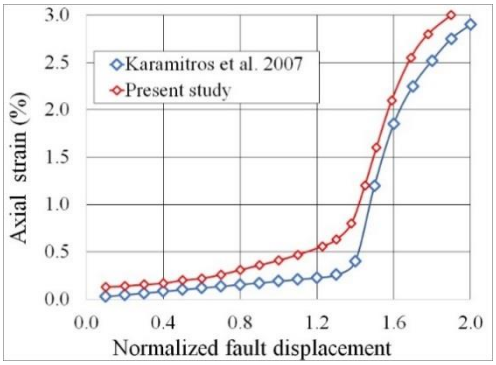

Fig. 6 Comparison of the analysis results for fault crossing angle of 45°

2.3 Verification

To validate the applied modeling, the results of the 3D non-linear numerical analyses of the steel pipelines at strike-slip fault crossing by Karamitros *et al.* (2007) has been used. For comparison, the response of a steel pipeline with external diameter of 0.9144 m and wall thickness of 0.0119 m has been used. The specification of the used steel and soil spring properties has been presented in Table 2.

The buried depth of the pipeline is 1.30 m in a medium-dense sand with internal friction angle (∅) of 36° and unit weight (γ) of 18 kN/m3. Also, the soil-pipeline interaction has been modeled by elastic-perfectly plastic axial, transverse horizontal and vertical soil springs. Fig. 6 shows

Table 2 Specification of the used steel and soil spring properties Karamitros *et al*. (2007)

API5L-X65 steel properties		
Yield stress (σ_1)	490 Mpa	
Failure stress (σ_2)	531 Mpa	
Failure strain (ε_2)	0.040	
Elastic Young modulus (E_1)	210 Gpa	
Yield strain ($\varepsilon_1 = \sigma_1/E_1$)	0.002	
Plastic Young modulus ($E_2=(\sigma_2 - \sigma_1)/(\varepsilon_2 - \varepsilon_1)$)	1.088 Gpa	
Soil spring properties		
	Yield force (kN/m)	Yield displacement (mm)
Axial (friction) springs	40.5	3.0
Transverse horizontal springs	318.6	11.4
Vertical springs (upward movement)	52.0	2.2
Vertical springs (downward movement)	1360.0	100.0

the comparison of the analysis results for fault crossing angle of 45°. Considering the differences in the modeling such as the application of the fully nonlinear analysis method and other modeling details in soil-structure interaction, the proximity of the results is reasonable.

3. Limit states for buried steel pipelines

Five common damage states due to the ground deformation for continuous pipelines are shell-mode buckling, pure tensile rupture, section ovalization, beam-mode buckling and flexural failure. In case of the strike-slip fault movement, the most frequently occurring failure modes for continuous pipelines assembled by welds as strong as or stronger than the pipe barrels are shell-mode buckling, pure tensile rupture and section ovalization (O'Rourke *et al.* 1990, Gresnigt and Karamanos 2009, Melissianos *et al.* 2020).

Investigations show that the local buckling strain is function of the D/t ratio, yield stress of the used steel type, internal/external pressure, manufacturing imperfections like deviation of the pipe walls from the perfect geometry and non-uniform compaction of the subsoil within the trench. With respect to the specification of X-grade steel types used in pipelines, the ultimate strain may reach to 21%. Nevertheless, due to the reasons like stress concentration and weld defect, more conservative values are considered in practice (EN 1998-4: 2006). While the tensile strain limits of 3% has been adopted by the EN 1998-4 provisions for seismic-fault- induced action on buried steel pipelines, the greater limit of 4% has been suggested by O'Rourke and Liu (1999). In this study, two values of 3% and 5% will be used as ultimate tensile strain capacity of continuous pipeline. The upper limit presents the slightly defected pipe with respect to the CSA Z662 (2007) pipeline design standard, Annex C.

Another important damage is cross-sectional flattening. It is not an ultimate state, but it can affect the serviceability. To keep the pipeline operational, the used ovalization limit state is as the following (NEN 3650: 2006)

$$\frac{\Delta D_{cr}}{D}=0.15 \quad (4)$$

4. Results and discussion

In this section, the results of the numerical analyses of the continuous steel pipeline are presented. The considered crossing angles are 30°, 45°, 70° and 90° with respect to the pipeline axis. The results are separately presented for pipeline embedded in two different clayey soils. Also, the effect of some parameters such as the D/t ratio, steel grades as well as the internal pressure on the pipeline response are studied. To check the sufficiency of the selected boundary conditions, several test analyses were performed. In these analyses, the affected length of the pipeline under the effect of the fault displacement were investigated for fixed and free conditions of the pipeline ends. The boundary condition at the pipeline end were considered similar to the soil boundary conditions at the models ends (as fixed).

4.1 Mechanical behavior of the non-pressurized (p=0) steel pipe

4.1.1 Stiff clay (D/t=72, p=0)

First, the response of the pipeline buried in the stiff clay with crossing angle of 45° is presented. Fig. 7 shows the overall deformation and longitudinal stress distribution of the pipeline with the increase in the fault movement. It is seen that at the small movement of the left block, the concentration of damage starts to develop around the crossing point. With the increase in the movement, along with the increase in the tension stress, the concentration of the longitudinal stress moves to the left. Also, this figure presents the affected length due to development of longitudinal stress. In the fault movement of 1 m, the longitudinal stress has extended to about 7 m at the right side while it is about 5 m at the left side (12 m in sum).

The pipeline response can also be investigated by the change in the pipe diameter. Fig. 8 shows the change in the

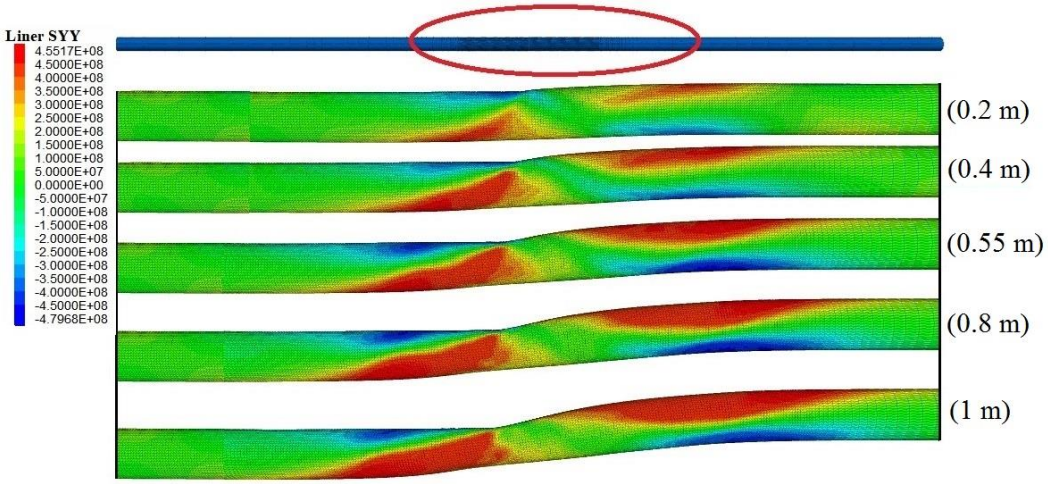

Fig. 7 Overall deformation and longitudinal stress distribution of the pipeline with the fault movement (stiff clay, X65, crossing angle of 45° and D/t=72)

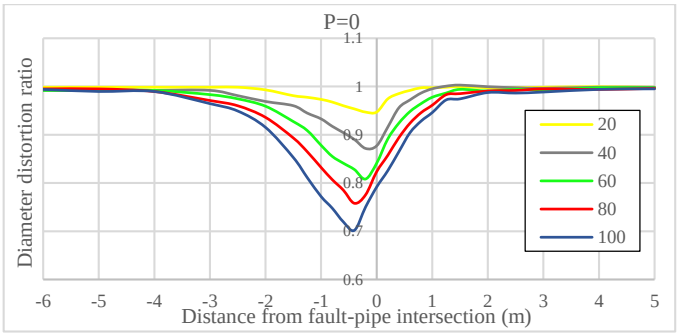

Fig. 8 Change in the ratio of the distorted pipe diameter to the initial diameter along the pipeline affected length (stiff clay, X65, crossing angle of 45° and D/t=72)

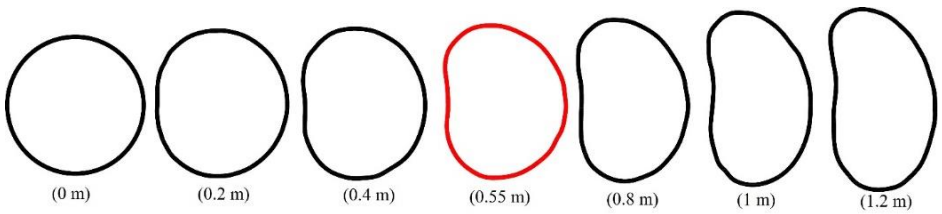

Fig. 9 Variation of the pipe cross-section at the most critical point for non-pressurized buried pipeline (stiff clay, X65, crossing angle of 45° and D/t=72)

ratio of the distorted pipe diameter to the initial diameter along the pipeline affected length. It is seen that the location of the maximum distortion ratio has moved 0.50 m to the left with the increase in the fault movement to 1 m. This happens due to the soil-pipe interaction and redistribution of stresses at this critical region. While the pipeline at right block is more affected by the longitudinal stress, the left side is affected by the change in the diameter. In this case, about 4 m of the pipeline length has undergone the cross-section distortion at the left block.

Also, in order to keep the pipeline operational, the correct estimation of the distorted cross-section is important. Fig. 9 presents the variation of the pipe cross-section at the critical point for crossing angle of 45° and non-pressurized condition. The cross-section under the fault movement of 0.55 m corresponds to the 15% cross-sectional flattening performance limit.

To see the mechanical behavior of the pipeline with respect to the performance criteria, the analyses results under the crossing angles of 30°, 45°, 70° and 90° have been presented in Fig. 10. In these set of analyses, the onset of the displacement of the pipeline wall at the area with maximum compression stress is considered as the local buckling. Also, in addition to the 3% and 5% tensile strain limits, the fault movements corresponding to the cross-sectional flattening limits of 15% and 30% are presented as well.

The circle symbol on the Fig. shows the occurrence of the buckling in the fault movement of 0.45 m. Also, the evolution of the local buckling with the increase in fault movement can be seen in Fig. 11. Since the soil pressure is applied from the back, the direction of the local buckling is inward.

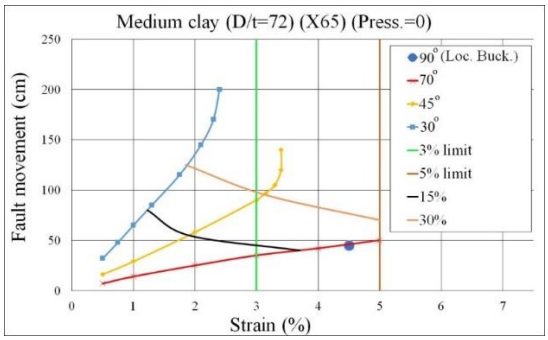

Fig. 10 Behavior of the pipeline at different fault crossing angles (stiff clay, X65, D/t=72 and p=0)

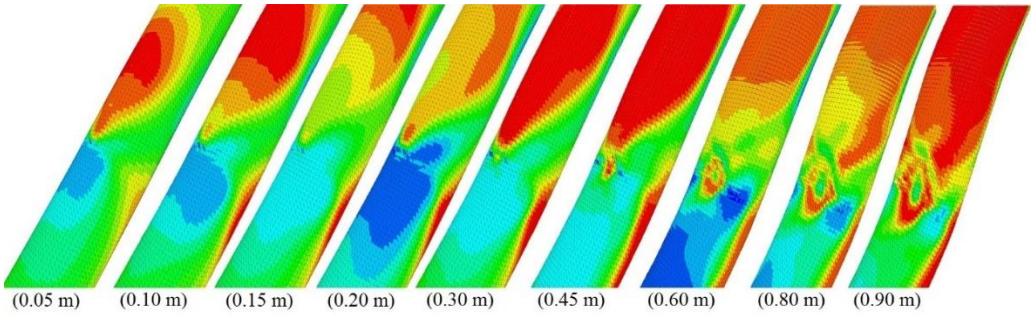

Fig. 11 Evolution of the local buckling with the increase in fault movement (stiff clay, X65, D/t=72 and p=0)

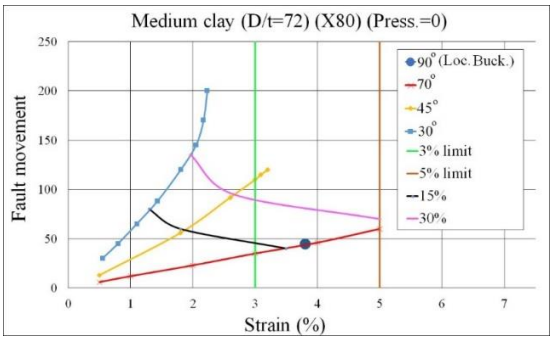

Fig. 12 Behavior of the pipeline at different fault crossing angles (stiff clay, X80, D/t=72 and p=0)

By the decrease in the crossing angle from 90° to 70°, more length of the pipeline is involved. The tensile and compression stresses are developed over greater length resulting no local buckling. In this case, the tensile strain increases rapidly with the increase in the fault movement so that it reaches to the limit value of 3% in 0.35 m. In the fault movement of about 0.40 m the cross-sectional limit of 15% is reached. With more increase, the tensile strain limit of 5% is reached in 0.50 m fault movement. For the milder crossing angles of 45° to 30°, there is an increase in the performance criteria as the result of the distribution of the tensile stress over greater pipeline length. The 15% cross-sectional distortion limit is reached before the tensile strain limits. While the 3% strain limit is reached at about 0.90 m for 45°, it doesn't reach for crossing angle of 30°.

4.1.2 Effect of the steel type (D/t=72, p=0)

Fig. 12 shows the mechanical behavior of the buried pipeline with X80 steel type. In the angle of 45°, a 0.3 m increase is seen for the 3% tensile strain limit. The tensile strain limits have not reached in in the angle of 30°, but the strains are smaller at similar fault movements. For the greater angles of 70° and 90°, although the performance limits are almost close, their strain values are different.

4.1.3 Effect of the soil type (D/t=72, p=0)

The mechanical behavior of the pipeline in soft clay for both X65 and X80 steel type are shown in Figs. 13 and 14.

The results show the increase in the performance limits with respect to the stiff clay case. The change in the soil type affects the smaller crossing angle more. Also, its effect on the pipeline with X80 steel type is greater with respect to the X65. For example, while there is an increase of 0.1m of fault movement in the 3% tensile strain limit for X65 steel type in 45°, it is about 0.3m for the X80 steel type.

For 30° crossing angle, although the tensile strain limits have not reached for both soil types, its value at similar ultimate fault movements is smaller for the pipeline in the soft clay soil. For example, the strain values at fault movement of 2m have decreased from 2.4% to 2% and

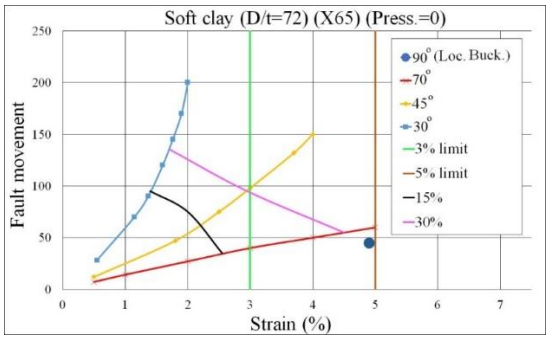

Fig. 13 Behavior of the pipeline at different fault crossing angles (soft clay, X65, D/t=72 and p=0)

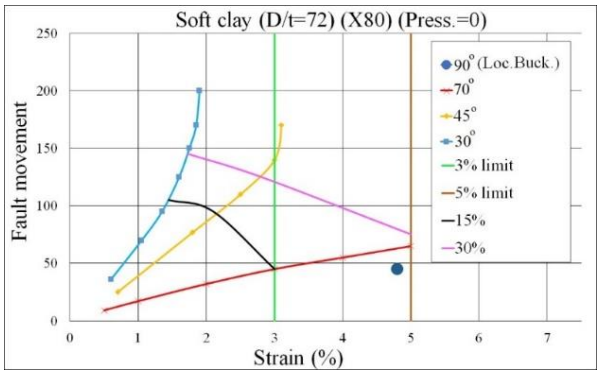

Fig. 14 Behavior of the pipeline at different fault crossing angles (soft clay, X80, D/t=72 and p=0)

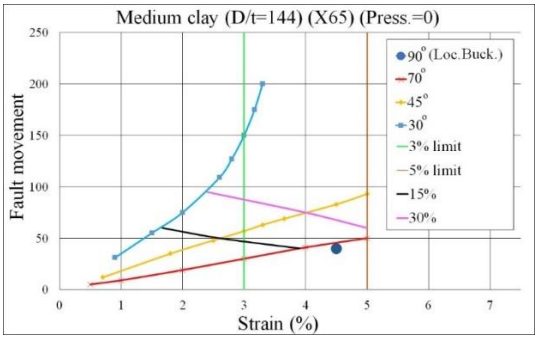

Fig. 15 Behavior of the pipeline at different fault crossing angles (stiff clay, X65, D/t=144 and p=0)

2.2% to 1.9% for X65 and X80 steel types, respectively. Likewise, the 15% cross-sectional flattening limits have increased from 0.8 m to 0.95 m and 0.85 m to 1.05 m for X65 and X80 steel types, respectively.

4.1.4 Effect of D/t (D/t=144, p=0)

Figs. 15-18 present the mechanical behavior of the pipelines with D/t of 144 buried in the different clays and steel types. The results show the decrease in the performance limits of the pipeline with D/t ratio of 144 with respect to the corresponding limit in 72. Also, the behavior of the pipelines with smaller crossing angles are affected more compared to the greater angles.

For example, while the tensile strain limit reaches to 2.4% at the fault movement of 2 m for pipeline with D/t ratio of 72 and steel type of X65 in crossing angle of 30°, it is about 3% at 1.5 m for the pipeline with D/t ratio of 144. A 0.2m and 0.3m decrease can also be seen for 15% and 30% cross-sectional flattening limit for this case. A 0.33 m and 0.35 m decrease in the 3% tensile strain limit is seen for the same case but with crossing angle of 45°. For the greater crossing angles, the effect of the change in D/t ratio is smaller. Its effect is generally limited to 0.05 m to 0.1 m for performance limits. It is noteworthy that the previously mentioned effects of the soil and steel type on the performance limits of the pipeline with D/t of 72 holds true for the D/t ratio of 144.

4.2 Mechanical behavior of the pressurized steel pipe

Since buried oil and gas steel pipeline operates under internal pressures, their mechanical behavior is quite different from those of the non-pressurized pipelines. The maximum operating pressure of the pipeline is the function of D/t and yielding stress. It is given as follows (ANSI/ASME B31.8: 2007)

$$p_{max} = 0.72 \times \left(2\sigma_y \frac{t}{D}\right) \quad (5)$$

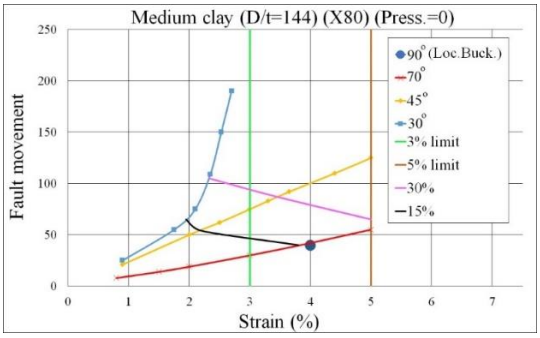

Fig. 16 Behavior of the pipeline at different fault crossing angles (stiff clay, X80, D/t=144 and p=0)

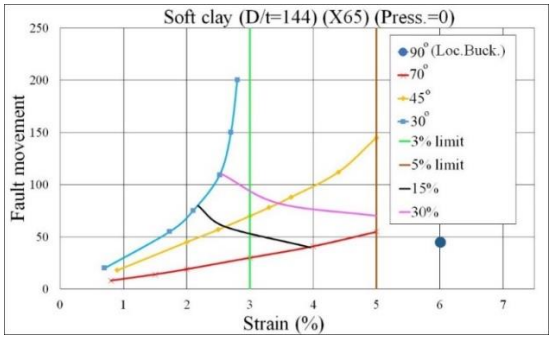

Fig. 17 Behavior of the pipeline at different fault crossing angles (soft clay, X65, D/t=144 and p=0)

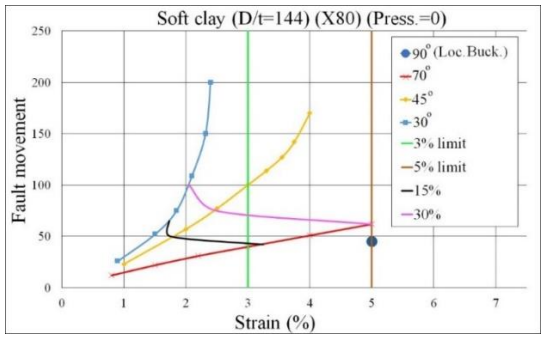

Fig. 18 Behavior of the pipeline at different fault crossing angles (soft clay, X80, D/t=144 and p=0)

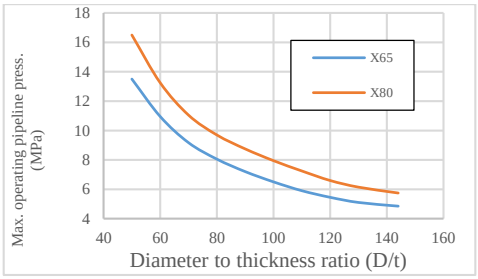

Fig. 19 Variation of maximum operating pipeline pressure with respect to D/t ratio

The variation of the maximum operating pipeline pressure with respect to D/t ratio has been presented in Fig. 19. In this section, the pipelines buried in different clayey soils with different steel types and D/t ratio are subjected to the 56% of the maximum internal pressure. The results are presented with respect to the pipeline damage limit states.

4.2.1 Behavior of the pressurized pipeline in stiff clay (D/t=72, p=0.56p_{max})

Fig. 20 shows the overall deformation and longitudinal stress distribution of the pressurized pipeline with the angle of 45° at different fault movements. It is seen that in the fault movement of 1.8 m the affected length by the longitudinal stress has increased to about 9 m at the right side while it has remained about 5 m at the left side (14 m in sum). Also, the location of the concentrated longitudinal stress moves to the left. To study the effect of the pipeline internal pressure on the pipe diameter, the change in the

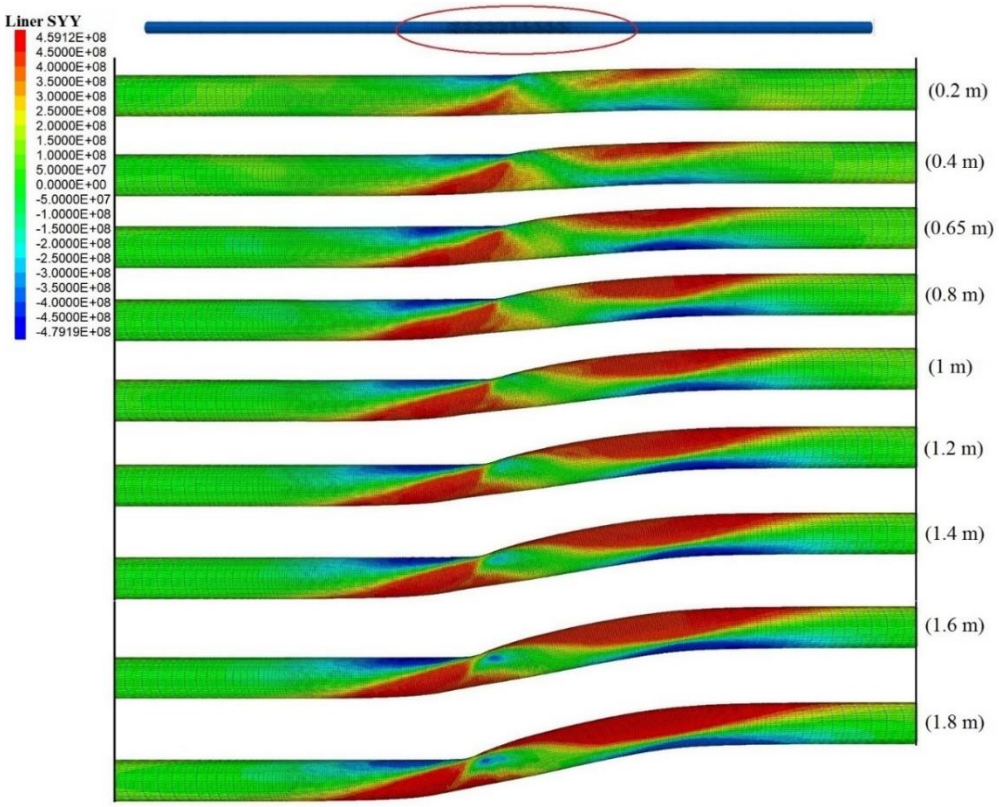

Fig. 20 Overall deformation and longitudinal stress distribution of the pipeline with the fault movement ($p=0.56p_{max}$, stiff clay, X65, crossing angle of 45° and D/t=72)

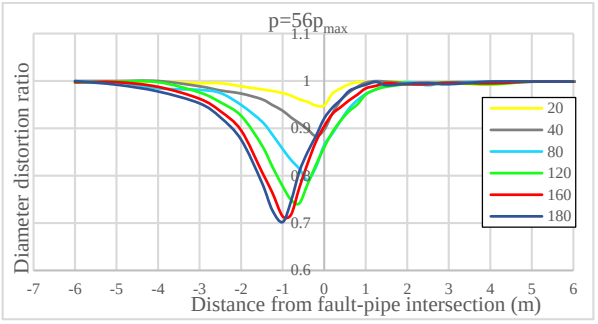

Fig. 21 Change in the ratio of the distorted pipe diameter to the initial diameter along the pipeline affected length ($p=0.56p_{max}$, stiff clay, X65, crossing angle of 45° and D/t=72)

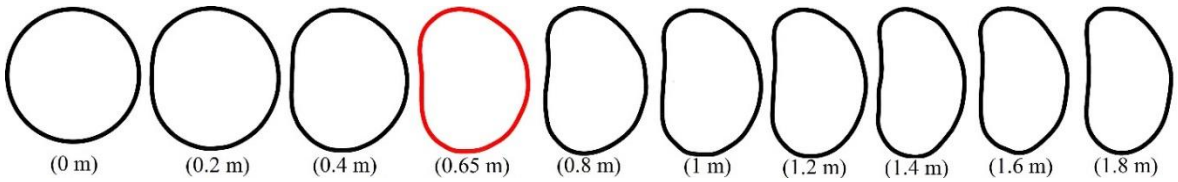

Fig. 22 Variation of the pipe cross-section at the most critical point for non-pressurized buried pipeline ($p=0.56p_{max}$, stiff clay, X65, crossing angle of 45° and D/t=72)

ratio of the distorted pipe diameter to the initial diameter along the pipeline affected length has been presented in Fig. 21. It indicates that the location of the cross-section with maximum distortion ratio has moved about 1.05 m to the left with the increase in the fault movement to 1.80 m; A 0.65 m increase with respect to the non-pressurized case. Also, Fig. 22 presents the variation of the pipe cross-section at the critical point for this case. The section marked with red corresponds to the 15% cross-sectional flattening performance limit. It has reached in about 0.10 m greater fault movement with respect to the non-pressurized case. Beyond the fault movement of 1 m, the change rate of the cross-section remains relatively constant. It is because the increase in the fault movement results in the increase in the tensile strain beyond this about 1m of the fault movement.

Fig. 23 shows the mechanical behavior of this pipeline

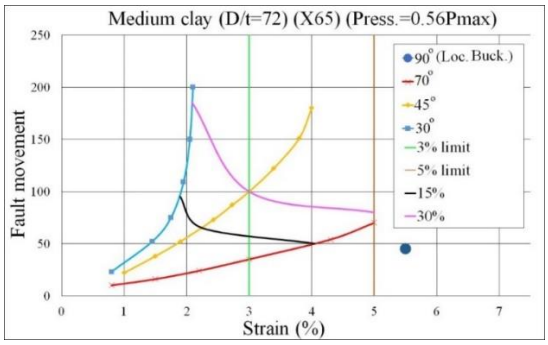

Fig. 23 Behavior of the pipeline at different fault crossing angles (stiff clay, X65, D/t=72, p=0.56p_{max})

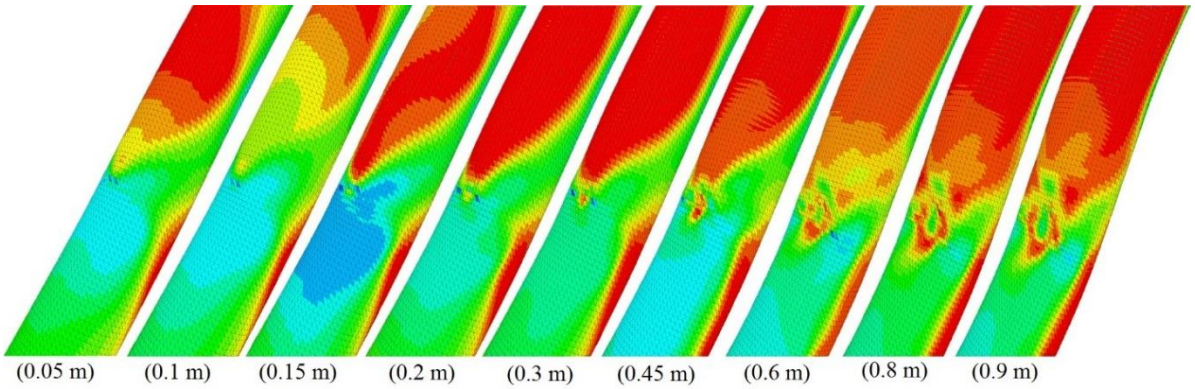

Fig. 24 Local buckling evolution by the increase in fault movement (p=056p_{max}, stiff clay, X65, D/t=72)

with respect to the performance criteria under different crossing angles. There is a significant increase in the performance limits of the X65 pressurized pipeline with 30° crossing angle with respect to the non-pressurized condition. The fault movement of 2 m has reached in smaller tensile strain. The cross-sectional flattening limits of 15% and 30% have reached in the greater fault movements of 0.15 and 0.60 m, respectively. In the crossing angle of 45°, there is an increase of 0.10 m in the fault movement resulting the tensile strain limits of 3%. In this crossing angle, the 5% tensile strain limit is not reached. While the pressurized pipeline reaches to 1.8 m of fault movement in the tensile strain of 4%, the non-pressurized pipeline's cross-section over-deformed in 1.2 m at 3.4% of tensile strain. The cross-sectional flattening limits of 15% and 30% have reached in the greater fault movements of 0.10 and 0.15 m, respectively. The effect of the internal pressure begins to decrease with the increase in the crossing angle. By the decrease in the crossing angle to 70°, despite the significant decrease in the performance limits of the pipeline, there is improvement with respect to the non-pressurized condition. There is a 0.20 m increase in the fault movement resulting tensile strain limit of 5%. Also, a 0.10 m increase in the cross-sectional flattening limit of 15% and 30% is seen. The results show that in case of the crossing angle of 90°, the local buckling occurs at about 0.45 m. The occurrence of the local buckling with the increase in fault movement has been presented for this case in Fig. 24.

Compared to the non-pressurized case, more improvement in the performance limits of the pressurized pipeline with X80 steel type is seen. As see in Fig. 25, the 2 m fault movement has reached in about 1.8% and 2.2% for pressurized and non-pressurized cases, respectively, with 30° crossing angle. The cross-sectional flattening limits of 15% and 30% have reached in the greater fault movements of 0.25 m and 0.65 m, respectively. In case of the 45°, there is a 0.35 m and 0.2 m improvement in the 3% tensile strain and 15% cross-sectional flattening limits, respectively, with respect to the non-pressurized condition. For this case, the 5% tensile strain limit has not reached in the fault movement of the 1.8 m. Small improvements is seen for greater crossing angles of 70° and 90°.

4.2.2 Behavior of the pressurized pipeline in soft clay (D/t=72, p=0.56pmax)

Figs. 26 and 27 present the mechanical behavior of the pressurized pipeline for X65 and X 80 steel types buried in soft clayey soil. The performance limits of the pipeline buried in the soft clayey has improved with respect to the corresponding pressurized pipe in stiff clayey soil as well as non-pressurized pipe in soft clayey soil. The best mechanical behavior among studied different conditions are seen in the pressurized pipeline with crossing angle of 30° in soft clayey soil. It is seen that the tensile strain limits are not reached meaning the control of the behavior by cross-sectional flattening limits. For these cases, the cross-sectional flattening limit of 15% occurs in the fault movement of 1.1 m and1.30 m for X65 and X80 steel type, respectively. In crossing angle of 45°, the increase in the fault movement resulting 3% tensile strain with respect to the non-pressurized condition reaches to about 0.3 m for both steel types. The cross-sectional flattening limit of 15% and 30% reaches in the greater fault movements of 0.15 m and 0.2 m for X65 and X80 steel types, respectively. Also,

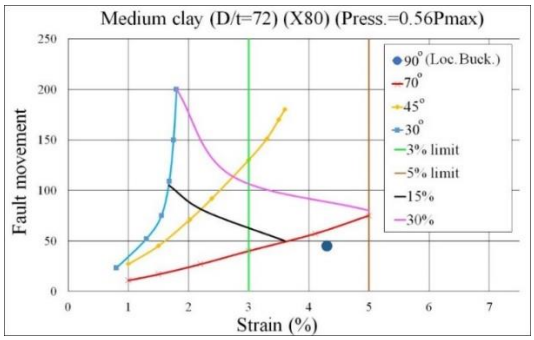

Fig. 25 Behavior of buried pipeline at different fault crossing angles (stiff clay, X80, D/t=72, p=0.56pmax)

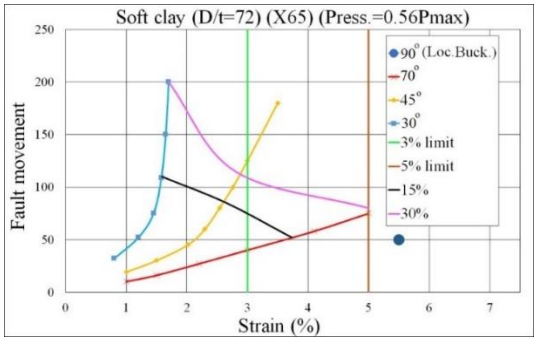

Fig. 26 Behavior of the buried pipeline at different fault crossing angles (soft clay, X65, D/t=72 and p=0.56p_{max})

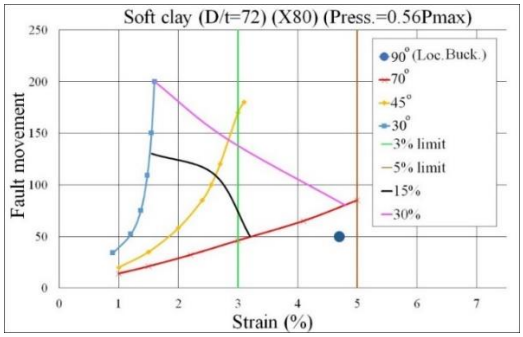

Fig. 27 Behavior of the buried pipeline at different fault crossing angles (soft clay, X80, D/t=72 and p=0.56p_{max})

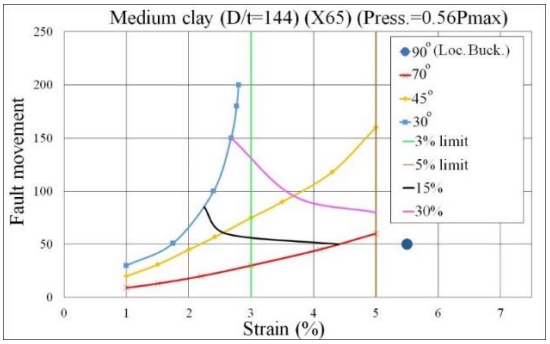

Fig. 28 Behavior of the buried pipeline at different fault crossing angles (stiff clay, X65, D/t=144 and p=0.56p_{max})

an increase of 0.25 m in the fault movement resulting 3% tensile strain is seen with respect to the similar condition in stiff clayey soil. The fault movement resulting the local buckling has reached to 0.50 m for both X65 and X80 steel types in 90° crossing angle. Almost similar improvement is seen for movement resulting 3% and 5% tensile strain limit for the crossing angle of 70°.

4.2.3 Behavior of the thin-walled pressurized pipeline (D/t=144, p=0.56p_{max})

Figs. 28-31 shows the analyses results of the pressurized pipeline with D/t of 144 under different fault crossing angles. It is seen that the performance limits of the pressurized thin-walled pipeline increase with respect to the corresponding non-pressurized cases. In the meantime,

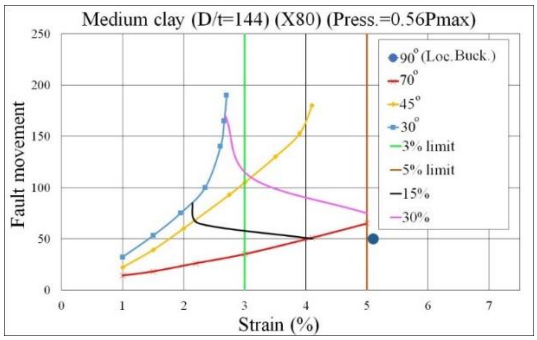

Fig. 29 Behavior of the buried pipeline at different fault crossing angles (stiff clay, X80, D/t=144 and p=0.56p_{max})

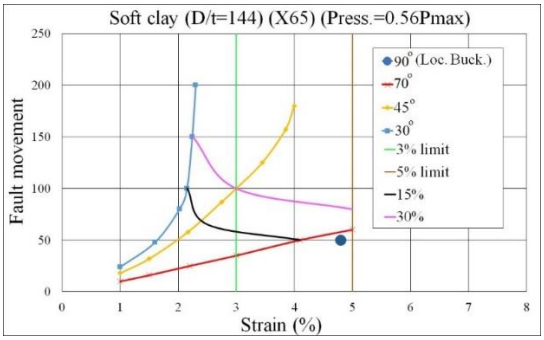

Fig. 30 Behavior of the buried pipeline at different fault crossing angles (soft clay, X65, D/t=144 and p=0.56p_{max})

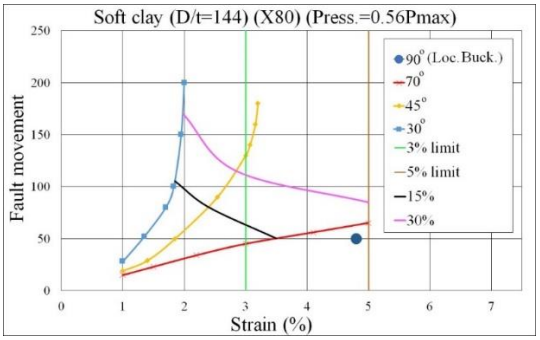

Fig. 31 Behavior of the buried pipeline at different fault crossing angles (soft clay, X80, D/t=144 and p=0.56p_{max})

there is a decrease with respect to the corresponding performance limits in D/t ratio of 72. For example, for the pipeline under the 45° crossing angle with X65 steel type buried in stiff clay, the tensile strain limits of 3% and %5 have reached in about 0.2m and 0.7m greater fault movements with respect to the similar non-pressurized condition.

Also, there is about 0.25 m decrease in the fault movements resulting 3% and 5% tensile strain limits with respect to the similar D/t ratio of 72 condition. The results show the decrease in the D/t effect by the increase in the crossing angle. There is a slight increase in the fault movement resulting the local bucking under the effect of the pressurized condition. It occurs in about 0.5 m of the fault movement.

5. Conclusions

Proper estimation of the pipeline response plays important role in mitigation studies. The lack of proper consideration of soil-pipeline interaction and prerequisites of the large strain level analysis leads to non-realistic pipeline deformation pattern. In this study, an advanced continuum modeling including material non-linearity in large strain deformation, hardening/softening soil behavior and soil-pipeline interaction is applied.

- The results showed the maximum affected length of about 20 meters for the studied conditions. Also, the affected length around the fault cutting plane is asymmetric. The ratio is about 35% for the fault moving block to 65% for the stationary part.
- To make the results useful in oil and gas engineering works, the fault movements corresponding to different damage limit states were presented. It was seen that while local buckling is the dominant damage state for greater crossing angle of 90°, other damage states become determining by the decrease in the crossing angle. In this case, the fault displacement causing local buckling varies from 0.4m to 0.55m by the change in

the factors like steel type and D/t ratio.

- The results show the increase in the pipeline affected length at the crossing angles other than 90°. While the tensile strain limit is the main damage state at the crossing angles of 70° and 45°, the cross-sectional flattening limit becomes the main damage state at the smaller 30° crossing angles. In the angle of the 30°, no tensile strain limit is reached at all. Based on the results, effect of the steel type is more evident at the crossing angles of 70° and 45° where the tensile strain limit is dominant. Its effect is more evident at the soft clayey soil. The main effect of the soil type was on the affected length of the pipeline resulting higher performance limits in softer one. Its effect reaches up to 40% in the fault movement resulting the 3% tensile strain limit (X80, 45° and D/t of 72). Although D/t ratio has got positive effect on the performance limits, it is not a major determining factor compared to other factors.
- In another part of this study, the behavior of the pipeline under 56% of the maximum internal pressure was separately investigated. The results show its positive effect more at 45° crossing angle where the tensile strain limit is determining. Its effect reaches up to about 40% compared to non-pressurized condition for some cases. Despite the smaller effect of the steel type under non-pressurized condition, the effect of this parameter increases under pressurized condition. Based on the results, the most effective factors on the pipeline performance are the crossing angle, pipe internal pressure, soil and steel type and D/t ratio, respectively.
- First, the presented behavior is limited to the steel pipeline crossing strike-slip fault. Also, the models represent the behavior of the continuous pipelines assembled by welds as strong as or stronger than the pipe barrels. The modeled pipeline diameter is about 914.4 mm. Although the effect of different pipeline wall thickness has been considered in this study, it doesn't necessarily represent the behavior of the pipelines with smaller diameters. Finally, the general mechanical behavior would be different in sandy soils to some extent.

References

Akbas. B., O'Rourke, M., Uckan, E., Shen, J. and Caglar, M. (2015), "Performance-based design of buried steel pipes at fault crossings", *Proceedings of the ASME 2015 Press. and Vessels & Piping Conf*, Boston, Massachusetts, USA, July.

Anastasopoulos, I., Gazetas, G., M, Bransby M.F., Davies M.C.R. and El Nahas, A. (2007), "Fault rupture propagation through sand: finite element analysis and validation through centrifuge experiments", *J Geotech Geo-environ Eng. ASCE*, **133**(8), 943-58. https://doi.org/10.1061/(ASCE)1090-0241(2007)133:8(943).

ANSI/API Spec 5L, Specification for line pipe (2007), 44th ed. American Petroleum Institute, USA.

ANSI/ASME B31.8 (2007), American Society of Mech Eng. Gas transmission and distribution piping systems.

Banushi, G., Squeglia, N. and Thiele, K. (2018), "Innovative analysis of a buried operating pipeline subjected to strike-slip fault movement", *Soil Dyn. Earthq. Eng.*, **107**, 234-249. https://doi.org/10.1016/j.soildyn.2018.01.015.

CSA-Z662 (2007), Canadian Standard Association, Oil and gas pipeline systems, Mississauga, Ontario, Canada.

Cundall, P.A. (2008), *FLAC3D Manual: a Computer Program for Fast Lagrangian Analysis of Continua (Version 4.0),* Minneapolis Uni., MN, USA.

Chaudhari, V., Kumar, V.D.K. and Kumar, R.P. (2013), "Finite element analysis of buried continuous pipeline subjected to fault motion", *Int. J. Struct. Eng.*, **4**(4), 314-331.

Cook, R.D., Malkus, D.S. and Plesha, M.E. (1989), *Concepts and Applications of Finite Element AnalysiS (3rd Ed.*, John Wiley & Sons, Inc., NY, USA.

Desmod, T.P., Power, M.S., Taylor, C.L. and Lau, R.W. (1995), "Behavior of large-diameter pipeline at fault crossings", *Proceedings of the 4. U.S. Conference on Lifeline Earthquake Engineering*, San Francisco, CA, USA, Aug.

Dey, S., Chakraborty, S. and Tesfamariam, S. (2020), "Structural performance of buried pipeline undergoing strike-slip fault rupture in 3D using a non-linear sand model", *Soil Dyn. Earthq. Eng.*, **135**, 106180. https://doi.org/10.1016/j.soildyn.2020.106180.

Erenson, C. and Terzi, N.U. (2022), "The effects of half-section waste tire reinforcement on pipe deformation behavior", *Geomech. Eng.*, **30**(6), 517-524. https://doi.org/10.12989/gae.2022.30.6.517.

EN 1998-4 (2006) Design of structures for earthquake resistance-Part 4: Silos, tanks and pipelines, Eurocode 8 (2003), European Committee for Standardization (CEN), Eur Comm Norm Brussels.

Gresnigt, A.M. and Karamanos, S.A. (2009), "Local buckling strength and deformation capacity of pipes", *Proceedings of the 19th International Offshore and Polar Engineering Conference*, Osaka, Japan, Jully.

Hashash, Y.M.A., Hook J.J., Schmidt, B. and I-Chiang Yao, J. (2001), "Seismic design and analysis of underground structures", *Tunn. Undergr. Sp. Tech.*, **16**, 247-293. https://doi.org/10.1016/S0886-7798(01)00051-7.

Joshi, S., Prashant, A., Deb, A. and Jain, S.K. (2011), "Analysis of buried pipelines subjected to reverse fault motion", *Soil Dyn. Earthq. Eng.*, **31**(7), 930–940. https://doi.org/10.1016/j.soildyn.2011.02.003.

Karamitros, D.K., Bouckovalas, G.D. and Kouretzis, G.P. (2007), "Stress analysis of buried steel pipelines at strike-slip fault crossings", *Soil Dyn. Earthq. Eng.*, **27**(3), 200-211. https://doi.org/10.1016/j.soildyn.2006.08.001.

Karamanos, S.A., Sarvanis, G.C., Keil, B.D. and Card, R.J. (2014), "Analysis and design of buried steel water pipelines in seismic areas", *J. Pipeline Sys. Eng. Pract.*, **8**(4), 04017018. https://doi.org/10.1061/(asce)ps.1949-1204.0000280.

Karamitros, D.K., Bouckovalas, G.D., Kouretzis, G.P. and Gkesouli, V. (2011), "An analytical method for strength verification of buried steel pipelines at normal fault crossings", *Soil Dyn. Earthq. Eng.*, **31**(11), 1452-1464. https://doi.org/10.1016/j.soildyn.2011.05.012.

Kaya, E.S., Uckan, E., Cakir, F. and Akbas, B. (2015), "A 3D nonlinear numerical analysis of buried steel pipes at strike-slip fault crossings", *Gradevinar*, **6**(8), 815-823. https://doi.org/10.14256/JCE.1317.2015.

Kennedy, R.P., Chow, A.W. and Williamson, R.A. (1977), "Fault movement effects on buried oil pipeline", *J. Transport. Eng. ASCE*, **103**, 617-633. https://doi.org/10.1061/TPEJAN.0000659.

Khoshghalb, A., Shafee, A. Tootoonchi, A., Ghaffaripour O. and Jazaeri S.A. (2020). "Application of the smoothed point interpolation methods in computational geomechanics: A comparative study", *Comput. Geotech.*, **126**, 103714. https://doi.org/10.1016/j.compgeo.2020.103714.

Kokavessis, N.K. and Anagnostidis, G.S. (2006), "Finite element modelling of buried pipelines subjected to seismic loads: soil structure interaction using contact elements", *Proceedings of the ASME PVP Conf*, Vancouver, BC, Canada, January.

Liu, A., Hu, Y., Zhao, F., Li, X., Takada, S. and Zhao, L. (2004), "An equivalent-boundary method for the shell analysis of buried pipelines under fault movement", *Acta Seismologica Sinica*, **17**(1), 150-156. https://doi.org/10.1007/s11589-004-0078-1.

Liu, M., Wang, Y.Y. and Yu, Z. (2008), "Response of pipelines under fault crossing", *Proceedings of the 18. International Offshore and Polar Engineering Conference*, Vancouver, BC, Canada, Jully.

MaCaffrey, M.A. and O'Rourke T.D. (1983), "Buried pipeline response to reverse faulting during the 1971 San Fernando Earthquake", *Proceedings of the ASME, PVP Conference*, USA.

Melissianos, V.E. and Gantes, C.J. (2017), "Numerical modeling aspects of buried pipeline-fault crossing", *Comput. Method. Earthq. Eng.*, **3**, 1-26. https://doi.org/10.1007/978-3-319-47798-5_1.

Melissianos, V.E., Vamvatsikos, D. and Gantes, C. (2020), "Methodology for failure mode prediction of onshore buried steel pipelines subjected to reverse fault rupture", *Soil Dyn. Earthq. Eng.*, **135**, 101-116. https://doi.org/10.1016/j.soildyn.2020.106116.

Mohitpour, M., Golshan, H. and Murray. A. (2007), *Pipeline Design & Construction: a Practical Approach*, (3rd Ed.), ASME Press, New York, NY, USA.

Morshed, A., Roy, K. and Hawlader, B. (2020), "Modeling of buried pipelines in dense sand for oblique movement in vertical - lateral plane", *J. Pipeline Sys. Eng. Pract.*, **11**(4), 04020050. https://doi.org/10.1061/(ASCE)PS.1949-1204.0000499.

NEN 3650 (2006), part-1: general, and part-2, Nederlands Normalisatie-Instituut. Requirements for pipelines systems steel pipelines, Nederlands.

Newmark, N.M. and Hall, W.J. (1979), "Pipeline design to resist large fault displacement", *Proceedings of the 1st National Commission on Excellence in Education*, DC, USA.

O'Rourke, M.J. (2009), "Wave propagation damage to continuous pipe", *Proceedings of the Tech. Counc. Lifeline Earthq. Eng. Conf. (TCLEE)*, Oakland, CA, USA, June-July. https://doi.org/10.1061/41050(357)76.

O'Rourke, T.D., Roth, B., Miura, F. and Hamada, M. (1990), "Case history of high-pressure pipeline response to liquefaction-Induced ground movements", *Proceedings of the 4th U.S. Natl. Conf. Earthq. Eng.,* Palm Springs, CA, USA, May.

O'Rourke, M.J. and Liu, X. (1999), *Response of Buried Pipelines Subject to Earthquake Effects*, Monograph series, Multidisciplinary center for earthquake engineering research, University of Buffalo, USA.

Ozcebe, A.G., Paolucci, R., Mariani, S. and Santoro, D. (2015), "A numerical study of the pressurized gas pipeline-normal fault interaction problem", *Proceedings of the 6th Int Conf on Earthq Geotech Eng*, Christchurch, New Zealand, November.

Rahman, M.A. and Taniyama, H. (2015), "Analysis of a buried pipeline subjected to fault displacement: A DEM and FEM study", *Soil Dyn. Earthq. Eng.*, **71**, 49-62. https://doi.org/10.1016/j.soildyn.2015.01.011.

Roudsari, M.T., Hosseini, M., Ashrafy. M., Azin, M., Nasimi, M., Torkaman, M. and Khorsandi, A. (2019), "New method to evaluate the buried pipeline–sandy soil interaction subjected to strike slip faulting", *J. Earthq. Eng.*, **26**(1), 89-112. https://doi.org/10.1080/13632469.2019.1662343.

Salehi Dezfooli, M., Khoshghalb A. and Shafee, A. (2022). "An automatic adaptive edge-based smoothed point interpolation method for coupled flow-deformation analysis of saturated porous media", *Comput. Geotech.*, **145**, 104672. https://doi.org/10.1016/j.compgeo.2022.104672.

Sarvanis, G.C. and Karamanos, S.A. (2017), "Analytical model for the strain analysis of continuous buried pipelines in geohazard areas", *Eng. Struct*,. **152**, 57-69. https://doi.org/10.1016/j.engstruct.2017.08.060.

Shafee, A. and Khoshghalb A. (2021), "An improved node-based smoothed point interpolation method for coupled hydro-mechanical problems in geomechanics", *Comput. Geotech.*, **139**, 104415. https://doi.org/10.1016/j.compgeo.2021.104415.

Shafee, A. and A. Khoshghalb (2022). "Particle node-based smoothed point interpolation method with stress regularisation for large deformation problems in geomechanics", *Comput. Geotech.*, **141**, 104494. https://doi.org/10.1016/j.compgeo.2021.104494.

Shi, J., Wang, J., Ji, X., Liu, H. and Lu, H. (2022), "Three-dimensional numerical parametric study of tunneling effects on existing pipelines", *Geomech. Eng.*, **30**(4), 383-392. https://doi.org/10.12989/gae.2022.30.4.383.

Shokouhi, S.K.S., Dolatshah, A. and Ghobakhloo, E. (2013), "Seismic strain analysis of buried pipelines in a fault zone using hybrid FEM-ANN approach", *Earthq. Struct*., **5**(4), 417-438. https://doi.org/10.12989/eas.2013.5.4.417.

Talebi, F. and Kiyono, J. (2021), "A refined nonlinear analytical method for buried pipelines crossing strike-slip faults", *Earthq. Eng. Struct. D.*, **50**, 2915-2938. https://doi.org/10.1002/eqe.3479.

Takada, S., Liang, J. and Li, T. (1998), "Shell-mode response of buried pipelines to large fault movements", *Struct Eng. JSCE*, **44**(A), 1637-1646.

Tohidi, R.Z. and Shakib, H. (2003), "Response of steel buried pipeline to the three-dimensional fault movements", *J Sci. Technol.*, **14** (56), 1127-1135.

Toprak, S., Çetin, O.A., Nacaroğlu, E. and Koç, A.C. (2010), "Pipeline performance under longitudinal permanent ground deformation", *Proceedings of the 14th ECEE*, Ohrid, Macedonia, March.

Trifonov, O.V. (2015), "Numerical stress-strain analysis of buried steel pipelines crossing active strike-slip faults with an emphasis on fault modeling aspects", *J. Pipeline Sys. Eng. Pract*., **6**(1), 1-10. https://doi.org/10.1061/(ASCE)PS.1949-1204.0000177.

Trifonov, O.V. and Cherniy, V.P. (2010), "A semi-analytical approach to a nonlinear stress-strain analysis of buried steel pipelines crossing active faults", *Soil Dyn. Earthq. Eng.*, **30**(11), 1298-1308. https://doi.org/10.1016/j.soildyn.2010.06.002.

Trifonov, O.V. and Cherniy, V.P. (2012), "Elastoplastic stress-strain analysis of buried steel pipelines subjected to fault displacements with account for service loads", *Soil Dyn. Earthq. Eng.*, **33**, 54-62. https://doi.org/10.1016/j.soildyn.2011.10.001.

Vazouras, P., Dakoulas, P. and Karamanos, S.A. (2015), "Pipe-soil interaction and pipeline performance under strike-slip fault movements", *Soil Dyn. Earthq. Eng.*, **72**, 48-65. https://doi.org/10.1016/j.soildyn.2015.01.014.

Vazouras, P. and Karamanos, S.A. (2017), "Structural behavior of buried pipe bends and their effect on pipeline response in fault crossing areas", *Bull. Earthq. Eng.*, **15**, 4999-5024. https://doi.org/10.1007/s10518-017-0148-0.

Vazouras. P., Karamanos, S.A. and Dakoulas, P. (2010), "Finite element analysis of buried steel pipelines under strike-slip fault displacements", *Soil Dyn. Earthq. Eng*., **30**(11), 1361-1376. https://doi.org/10.1016/j.soildyn.2010.06.011.

Vazouras, P., Karamanos, S.A. and Dakoulas, P. (2012), "Mechanical behavior of buried steel pipes crossing active strike-slip faults", *Soil Dyn. Earthq. Eng.*, **41**(11), 164-180. https://doi.org/10.1016/j.soildyn.2012.05.012.

Wang, L.R.L. and Yeh, Y.A. (1985), "A refined seismic analysis and design of buried pipeline for fault movement", *Earthq. Eng. Struct. D.*, **13**, 75-96. https://doi.org/10.1002/eqe.4290130109.

Xu, J. and She, G. (2022), "Thermal post-buckling analysis of porous functionally graded pipes with initial geometric imperfection", *Geomech. Eng.*, **31**(3), 329-337. https://doi.org/10.12989/gae.2022.31.3.329.

Yigit, A. (2022), "Response of segmented pipelines subject to earthquake effects", *Geomech. Eng.*, **30**(4), 353-362. https://doi.org/10.12989/gae.2022.30.4.353.

GC